Neurobiology of Disease 132 (2019) 104583

Contents lists available at ScienceDirect

Neurobiology of Disease

journal homepage: www.elsevier.com/locate/ynbdi

Transcriptomes of Dravet syndrome iPSC derived GABAergic cells reveal dysregulated pathways for chromatin remodeling and neurodevelopment

Jens Schuster[a,*,1], Loora Laan[a,1], Joakim Klar[a,1], Zhe Jin[b], Mikael Huss[c], Sergiy Korol[b], Feria Hikmet Noraddin[a], Maria Sobol[a], Bryndis Birnir[b], Niklas Dahl[a,*]

[a] Department of Immunology, Genetics and Pathology, Science for Life Laboratory, Uppsala University, Biomedical Centre, Box 815, 751 08 Uppsala, Sweden
[b] Department of Neuroscience, Uppsala University, Uppsala, Sweden
[c] Wallenberg long-term Bioinformatics Support, Science for Life Laboratory, Department of Biochemistry and Biophysics, Stockholm University, Stockholm, Sweden

ARTICLE INFO

Keywords:
Dravet syndrome
SCN1A
$Na_v1.1$
iPSC
Neural differentiation
Neurodevelopment
Chromatin architecture

ABSTRACT

Dravet syndrome (DS) is an early onset refractory epilepsy typically caused by de novo heterozygous variants in *SCN1A* encoding the α-subunit of the neuronal sodium channel $Na_v1.1$. The syndrome is characterized by age-related progression of seizures, cognitive decline and movement disorders. We hypothesized that the distinct neurodevelopmental features in DS are caused by the disruption of molecular pathways in $Na_v1.1$ haploinsufficient cells resulting in perturbed neural differentiation and maturation. Here, we established DS-patient and control induced pluripotent stem cell derived neural progenitor cells (iPSC NPC) and GABAergic interneuronal (iPSC GABA) cells. The DS-patient iPSC GABA cells showed a shift in sodium current activation and a perturbed response to induced oxidative stress. Transcriptome analysis revealed specific dysregulations of genes for chromatin structure, mitotic progression, neural plasticity and excitability in DS-patient iPSC NPCs and DS-patient iPSC GABA cells versus controls. The transcription factors FOXM1 and E2F1, positive regulators of the disrupted pathways for histone modification and cell cycle regulation, were markedly up-regulated in DS-iPSC GABA lines. Our study highlights transcriptional changes and disrupted pathways of chromatin remodeling in $Na_v1.1$ haploinsufficient GABAergic cells, providing a molecular framework that overlaps with that of neurodevelopmental disorders and other epilepsies.

1. Introduction

Dravet syndrome (DS) is a devastating type of epilepsy with an unfavorable long-term outcome and pharmaco-resistance (Akiyama et al., 2010; Brunklaus and Zuberi, 2014; Delahaye-Duriez et al., 2016; Symonds et al., 2017). The onset of seizures, usually triggered by fever, occurs within the first 12 months of life. The symptoms progress with age including increased seizure frequency, neurodevelopmental delay, age-dependent movement disorders and behavioral problems (Catarino et al., 2011; Dravet et al., 2005, 2011) suggesting pathophysiological mechanisms that interfere with brain development. Approximately 80% of Dravet cases are caused by heterozygous *SCN1A* gene variants resulting in $Na_v1.1$ haploinsufficiency (Bechi et al., 2012; Chopra and Isom, 2014; Depienne et al., 2009; Harkin et al., 2007; Lorincz and Nusser, 2010; Scheffer et al., 2009).

Important prior insights into DS neuropathogenesis have come from studies of *Scn1a* heterozygous mouse models showing loss of sodium current in GABAergic inhibitory interneurons (Yu et al., 2006) and prolonged circadian rhythms (Kalume et al., 2015). In addition, several groups have modeled DS using patient derived human induced pluripotent stem cells (iPSC) to recapitulate disease mechanisms (Higurashi et al., 2013; Jiao et al., 2013; Maeda et al., 2016; Schuster et al., 2015; Sun et al., 2016). These studies have confirmed partial or delayed sodium currents of activated inhibitory but not excitatory neurons (Higurashi et al., 2013; Jiao et al., 2013; Maeda et al., 2016), supporting the notion that seizures in DS are caused by deficient cortical inhibition (Sun et al., 2016). While it is clear that heterozygous *SCN1A* variants cause a reduced sodium current density, the biological processes and the molecular mechanisms behind the different neuropathological features in DS are not fully understood. Furthermore, only a few studies have analyzed the effect of *SCN1A* variants in iPSC derivatives enriched for cortical GABAergic neurons, the cell type believed to mediate the abnormalities in DS (Catterall et al., 2010; Higurashi et al., 2013; Jiao et al., 2013; Lorincz and Nusser, 2010;

* Corresponding authors.
E-mail addresses: jens.schuster@igp.uu.se (J. Schuster), niklas.dahl@igp.uu.se (N. Dahl).
[1] These authors contributed equally to this work.

https://doi.org/10.1016/j.nbd.2019.104583
Received 23 October 2018; Received in revised form 31 July 2019; Accepted 20 August 2019
Available online 21 August 2019
0969-9961/

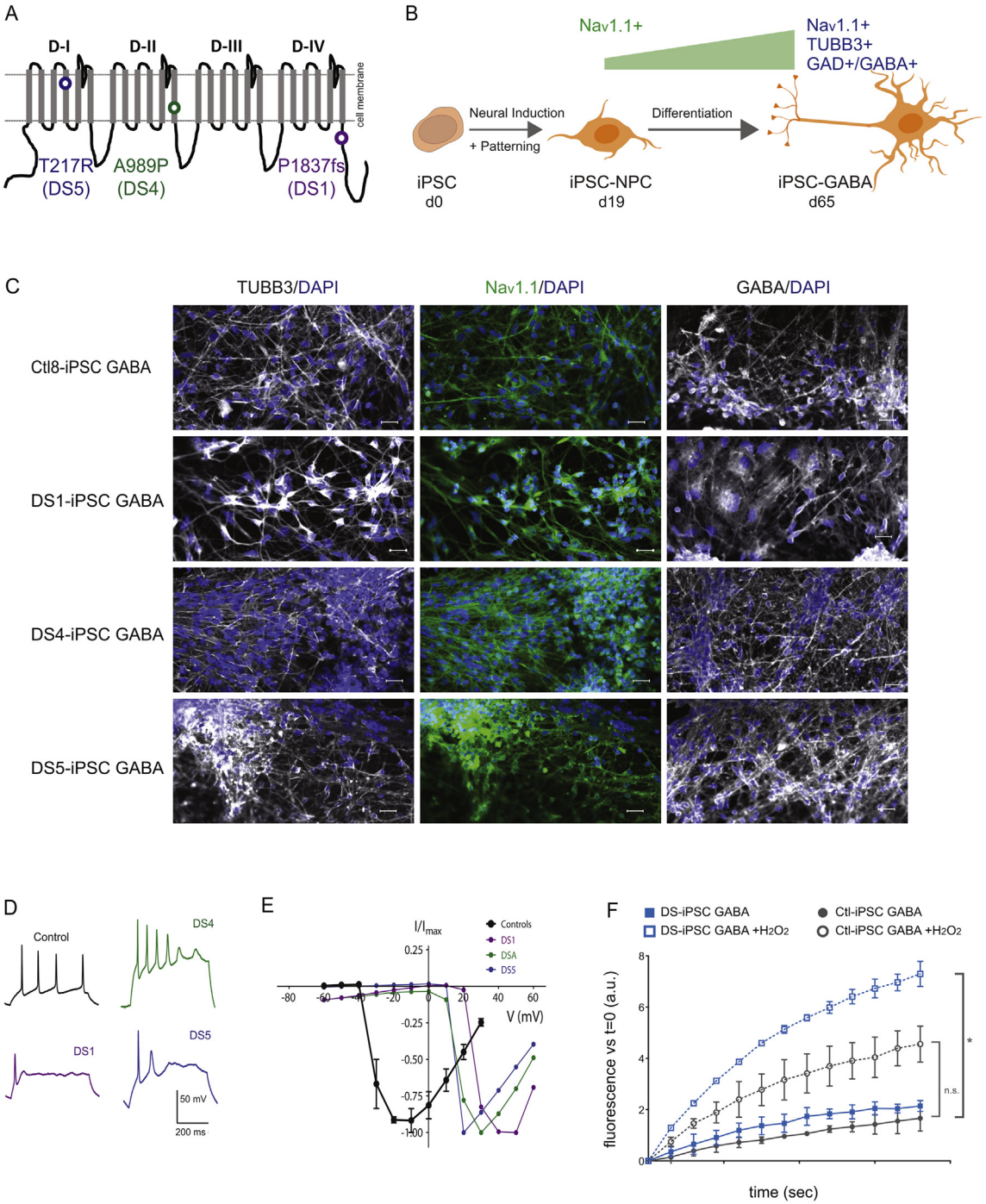

Fig. 1. DS-iPSC GABAergic cells with *SCN1A* variants exhibit impaired sodium current activation and stress response.
A, Schematic structure of *SCN1A* encoded voltage-gated sodium channel (Na_v) 1.1 consisting of four transmembrane domains (D-I to D-IV) and an intracellular C-terminal tail. The predicted Na_v 1.1 protein alterations caused by pathogenic *SCN1A* variants in three patients with DS are indicated (DS1: p.P1837fs, purple, within the intracellular tail region; DS4: p.A989P, green, located in the pore region of domain 2 segment 6 (D-II-6); DS5: p.T217R, blue, within the voltage sensor region of domain 1 segment 4 (D-I-6)). **B**, Schematic outline of protocol used to differentiate iPSCs into neural cultures enriched for GABAergic cells. Neural markers stained positive are indicated (NPC: Neural progenitor cells). **C**, Neural cultures at d65 are highly enriched for cells with a cortical interneuron identity. Immunostaining of iPSC-GABA cells at d65 derived from subjects Ctl8 (healthy donor), DS1, DS4 and DS5, respectively, against β-III-tubulin (TUBB3), γ-butyric acid (GABA) and Na_v1.1 counterstained with DAPI. Size bars: 20 µm. **D**, Action potentials (AP) evoked in response to step current injections in Ctl-iPSC GABA (control) and DS-iPSC GABA cells containing each of the three *SCN1A* variants (DS1, DS4 and DS5), respectively. Representative and aberrant responses to step current injections are shown for cells from each of the three DS-iPSC GABA cultures. The holding potential was −60 mV and a 40 pA step current injection lasting 500 ms was applied. **E,** DS-iPSC GABA cells show a shift in sodium current activation. Current-voltage relationship for Ctl-iPSC GABA (black) and DS-iPSC GABA cells (DS1, purple; DS4, green; DS5, blue). Representative currents are shown for individual DS-iPSC GABA cells and an average current for control cells ($n = 3$). DS-iPSC GABA cells display a shift of sodium current activation to more depolarized potentials as compared to the Ctl-iPSC GABA cells suggesting specific deficits in sodium currents (error bars represent SEM; V, voltage (mV); I, current (mA); controls, black; DS1, purple; DS4, green; DS5, blue). **F**, Increased sensitivity to cellular stress in DS-iPSC GABA cells. Analysis of intracellular reactive oxygen species (ROS) in iPSC GABA at d65 with (open symbols) or without (closed symbol) induction using hydrogen peroxide (H_2O_2). Increased ROS levels are detected in DS-iPSC GABA cells ($n = 3$) carrying pathogenic *SCN1A* variants after H_2O_2 induction (blue squares) when compared to Ctl-iPSC GABA cells ($n = 3$; grey circles; * $p < .05$; one-way ANOVA and Kruskal Wallis ad hoc test). (For interpretation of the references to colour in this figure legend, the

reader is referred to the web version of this article.)

Maeda et al., 2016; Yu et al., 2006).

Transcriptional signatures have uncovered critical molecular networks and disrupted functions in neurodevelopmental disease (Katayama et al., 2016; Tebbenkamp et al., 2014). Given the extended maturation of the human GABAergic system from late gestation into postnatal stages (Xu et al., 2011), we therefore set out to decipher abnormalities in the gene expression profile in DS-patient iPSCs at two different time points along neural differentiation into GABAergic cells. Here, we generated DS patient iPSC neural progenitor cells (DS-iPSC NPC) and DS patient iPSC GABAergic cells (DS-iPSC GABA) derived from three patients with different *SCN1A* variants. Using RNA sequencing, we characterized the gene expression profiles of iPSC neural lines derived from the DS patients and three healthy control subjects. Moreover, we assessed electrophysiological properties and sensitivity to cellular stress of DS-iPSC GABA cells versus control cells. Taken together, we demonstrate that DS-iPSC GABA cells with characteristic electrophysiological abnormalities show increased sensitivity to induced stress and dynamic dysregulations of specific molecular pathways and genes, providing a transcriptional framework relevant for the complex neuropathophysiology of DS.

2. Materials and methods

2.1. Patient characteristics and sampling

We identified three patients (DS1, DS4 and DS5) with clinical features of DS. The three patients had an onset of generalized febrile seizures within the first ten months of life. Patient DS1 was diagnosed with DS, severe developmental delay and ataxia. The patient carries a de novo frameshift variant c.5502-5509dupGCTTGAAC (p.Pro1837Argfs24) in the intracellular COOH-terminal domain of $Na_v1.1$. Patient DS4, diagnosed with DS and developmental delay, carries a de novo pathogenic missense variant c.2965G > C (p.Ala989Pro), located in the pore region of the second transmembrane domain of the $Na_v1.1$ protein (domain II, segment 6). Patient DS5 had a less severe DS phenotype presenting with mild cognitive decline and she had a history of both febrile and non-febrile seizures. The patient carries a pathogenic missense variant c.651C > G (p.Thr217Arg; domain I segment 4, voltage sensor of $Na_v1.1$) inherited from her mother with FS+ (Fig. 1A; Supplementary Fig. S1A). Dermal fibroblast (HDF) lines were established from skin punch biopsies obtained from each patient (Rooney and Czepulkowski, 1992). All procedures were in accordance with the Helsinki convention and written informed consent was obtained from all patients or their legal guardians. The study was approved by the regional ethical committee of Uppsala, Sweden (D-numbers 319/2009 and 209/2016).

2.2. Cell reprogramming and stem cell culture

Fibroblasts obtained from skin punch biopsies were maintained in human foreskin fibroblast (HFF) medium [Dulbecco's modified Eagle's medium (DMEM, high glucose; Sigma) supplemented with 10% fetal bovine serum (FBS; Sigma), 2 mM L-glutamine, non-essential amino acids, and penicillin/streptomycin (Life Technologies)] in a humidified atmosphere with 5% CO_2 at 37 °C. Fibroblasts from DS patients ($n = 3$) and healthy control subjects (n = 3) were reprogramed using the Cytotune® iPS 2.0 kit (ThermoFisher Scientific) following manufacturer's protocols with minor modifications. Briefly, 25′000 fibroblasts were plated per 1-well of a 24-well plate (Sarstedt) and kept in HFF medium for additional two days and transduced by Sendai virus expressing the four factors OCT4, SOX2, KLF4 and c-MYC (CytoTune®-iPS Sendai Reprogramming Kit, Gibco). On day 3 after transduction, cells were plated into 2 wells of a Matrigel® (BD) coated 6-well plate in TesR™-E7™ medium (Stem Cell Technologies). Medium was changed daily until distinct iPSC colonies appeared (day 21–30; Supplementary Fig. S1B). The iPSCs colonies were picked manually and transferred to Vitronectin XF™ (VTN-N, Stem Cell Technologies) coated plates and further expanded in Essential-8™ medium (ThermoFisher Scientific). Three control iPSC lines (Ctl1, Ctl7 and Ctl8) were derived from healthy subjects and have been described earlier (Sobol et al., 2015). All six iPSC lines were maintained on Vitronectin coated cell culture ware in Essential-E8™ medium (ThermoFisher Scientific) and passaged as clumps with gentle cell dissociation reagent (GCDR; Stem Cell Technologies).

2.3. Sanger sequencing

The presence of heterozygous *SCN1A* variants were confirmed in fibroblasts and iPSCs lines derived from DS patients by bidirectional sequencing of PCR products using primers flanking each *SCN1A* variant (Supplementary methods).

2.4. Cortical differentiation

Cortical differentiation of iPSC was carried out as described (Maroof et al., 2013)Fig. 1B; Supplementary Fig. S2A). Two days before neural induction, cells were harvested with GCDR and plated in Essential-E8™ medium supplemented with 10 μM Rho-kinase inhibitor Y27632 (Stem Cell Technologies) to Matrigel® coated 6-well culture dish to yield > 80% confluence the next day. When cells reached 100% confluence, neural differentiation was induced on iPSC (day 0) using dual SMAD inhibition. Briefly, cells were washed with 1× DPBS and neural induction medium (NIM; [DMEM-KO, 15% KnockOut Serum Replacement, 1× GlutaMax, 1× non-essential amino acids, 1% penicillin/streptomycin (all Invitrogen)]), supplemented with 2 μM tankyrase inhibitor XAV939 (Sigma), 100 nM ALK2/3 inhibitor LDN193189 (Miltenyi Biotech) and 10 μM ALK4/5/7 inhibitor SB431542 (Millipore) was added. Medium was changed on day (d) 1 and d2. On d4, medium was replaced by NIM:NBN medium [Neurobasal medium, N2 (1:100), B27 without Vitamin A (1:200), 1% penicillin/streptomycin (all Invitrogen)] in a ratio of 3:1, supplemented with inhibitors as in the induction medium. Medium was changed on day 6 (NIM:NBN; 1:1) and d8 (NIM:NBN; 1:3). On d10 of neural differentiation, cells were harvested with accutase® (Sigma), collected by centrifugation, washed in DPBS, and subsequently spotted or plated at a density of 80–100,000 cells/cm^2 onto poly-L-ornithine (PLO)/laminin (LMN; both Sigma) coated plates or cover slips, respectively. From d10, cells were patterned towards cortical fate using NBN medium supplemented with 5 nM recombinant mouse sonic hedgehog (SHH C25II; RnD Systems), 1 μM SHH agonist Purmorphamine (Miltenyi biotech), 10 ng/ml recombinant human brain derived neurotrophic factor (BDNF; ThermoFisher Scientific), 200 μM ascorbic acid (Sigma) and 100 μM 2′-O-Dibutyryladenosine 3′,5′-cyclic monophosphate (cAMP; Sigma). Medium was changed on d13 and d16. On d19, cells obtained neuronal progenitor cells (iPSC NPC) morphology and were plated onto PLO/LMN coated coverslips/dishes in NBN medium supplemented with BDNF, ascorbic acid and cAMP. For further differentiation, medium was changed twice a week from this point onwards until cells were either harvested, fixed with 4% PFA or analyzed at > d65 (iPSC GABA).

2.5. In vitro differentiation of embryoid bodies

Embryoid bodies (EBs) were formed in AggreWell™ EB formation medium (Stem Cell Technology) using AggreWell™ 400 Plates (Stem Cell Technologies) following manufacturer's protocol. Two days after EB harvest, AggreWell™ EB formation medium was replaced by fresh

medium and two days later, an equal volume of KSR medium (DMEM Knock-out, supplemented with 15% serum replacement, non-essential amino acids, L-glutamine, penicillin/streptomycin (all ThermoFisher Scientific)) was added. After two days, medium was changed and EBs were cultured as floating spheres for a total of four weeks. EBs were harvested for RNA isolation and total RNA was analyzed by scorecards (ThermoFisher Scientific).

2.6. RNA isolation, quantitative real-time RT/PCR and RNA sequencing

Total RNA from iPSC, EBs, iPSC NPCs and iPSC GABA cells was isolated using a miRNeasy micro kit (Qiagen) following manufacturer's protocol. Quality of RNA was assessed using a RNA 6000 Nano Chip and a Bioanalyzer (Agilent Technologies) and RNA samples with an integrity number (RIN) above 7.7 were accepted for further analysis. For quantitative real-time RT/PCR (qPCR), 1 µg RNA was reverse-transcribed into cDNA using SuperScript VILO cDNA Synthesis Kit (ThermoFisher Scientific). FastStart Universal SYBR Green Master mix (Roche) was used for qPCR with relevant primers (Supplementary Table S1). The PCR mix for a 25 µl reaction contained 12.5 µl FastStart Universal SYBR Green Master Mix, 300 nM of forward and reverse primer and 2.5 µl of template cDNA. StepOnePlus™ Real-Time PCR System (Applied Biosystems) and Step one software v2.2.2 were employed and results were normalized to GAPDH. Paired-end RNA-sequencing libraries were prepared from 350 µg of total RNA using TruSeq stranded total RNA library preparation kit with RiboZero Gold treatment (Illumina) according to manufacturer's protocols. Sequencing was performed on a HiSeq2500 (Illumina) with v4 sequencing chemistry on a total of 2 lanes at the SNP&SEQ platform, Science for Life Laboratory, Uppsala, Sweden.

2.7. Characterization of iPSCs and EBs using TaqMan™ hPSC Scorecard™

Pluripotency and germ-layer formation were assessed in all six iPSC lines and after differentiation into EBs. One µg of total RNA was converted to cDNA using a High capacity cDNA Synthesis kit (ThermoFisher Scientific), subsequently mixed with TaqMan™ Gene Expression Master Mix, and loaded onto a TaqMan™ hPSC Scorecard™ (ThermoFisher Scientific) following manufacturer's protocols. The scorecard was run on a 7900HT Real-Time PCR System (Applied Biosystems), and data was analyzed using the web-based analysis interface (www.thermofisher.com).

2.8. Immunofluorescence staining (IF)

Immunostaining was performed on cells fixed with ice-cold 4% paraformaldehyde and subsequent permeabilization in blocking solution (1 × phosphate-buffered saline pH 7.4, 1% bovine serum albumin, 0.1% Triton X-100, 5% donkey serum (all Sigma)). Primary antibodies used for immunostaining were GABA (1:500, Sigma), $Na_v1.1$ (1:40, Abcam), β-III Tubulin (1:10,000, Sigma), NANOG (1:100, Millipore), TRA-1-60 (1:100, Thermo), SSEA4 (1:100, Thermo). Primary antibodies were allowed to bind overnight separately or in appropriate combinations at 4 °C. After washing three times in 1 × TBS, 0.05% Tween, the secondary antibodies donkey anti-goat IgG AlexaFluor 633, donkey anti-rabbit IgG AlexaFluor 568 or donkey anti-mouse IgG AlexaFluor 488 (1:1000; Invitrogen) were applied alone or in appropriate combinations for 1.5 h at room temperature in the dark. Visualization was performed on a Zeiss 510 confocal microscope (Carl Zeiss Microscopy) using Zen imaging software, or an AxioImager (Zeiss), respectively.

2.9. Karyotyping

Chromosome preparation of iPSCs was performed as described previously (Sobol et al., 2015). Metaphases of G-banded chromosomes (> 400 bands) were analyzed using Metafer slide scanning platform and IKAROS-software (MetaSystems). Twenty metaphases were analyzed for each cell line.

2.10. Analysis of ROS levels in iPSC derived GABAergic neuronal cells

Reactive oxygen species (ROS) levels in cultured neuronal cells were analyzed using the OxiSelect™ Intracellular ROS Assay Kit (Cell Biolabs) following manufacturer's protocol. Briefly, DS-iPSC GABA and Ctl-iPSC GABA cells at d65 were loaded with 2′,7′-dichlorodihydrofluorescin diacetate (DCFH-DA) for 1 h. The levels of reactive oxygen species (ROS) were determined from the increase in fluorescence (excitation: 480 nm; emission: 530 nm) for 120 min using a VarioScan LUX (ThermoFisher Scientific) plate reader. A second set of cells was treated with hydrogen peroxide immediately before fluorescence measurement. Data was normalized to fluorescence at start of the experiment ($t = 0$) and plotted as relative fluorescence units using Prism® reflecting change of intracellular ROS load over time.

2.11. Electrophysiological recordings of GABAergic neural cells

Whole-cell patch-clamp recordings were performed on DS-iPSC GABA and Ctl-iPSC GABA cells from d65 at room temperature (20–22 °C) with Axopatch 200B amplifier, filtered at 2 kHz, digitized on-line at 10 kHz using an analogue-to-digital converter and pClamp 10.2 software (Molecular Devices, USA) as described (Jin et al., 2011). Recording pipettes were made from borosilicate glass capillaries (Harvard Apparatus LTD, UK) with a resistance between 4 and 8 MΩ when filled with 3.2 µl of intracellular solution. The intracellular solution contained 130 mM K-Gluconate, 20 mM KCl, 0.3 mM NaGTP, 0.2 mM EGTA, 4 mM MgATP, 10 mM HEPES, 10 mM Na-phosphocreatine adjusted to pH 7.3 with KOH (all from Sigma-Aldrich), 285 mOsm. The extracellular solution contained 140 mM NaCl, 5 mM KCl, 2 mM $CaCl_2{\cdot}2H_2O$, 2 mM $MgCl_2{\cdot}6H2O$, 10 mM HEPES and 10 mM glucose adjusted to pH 7.4 with NaOH (all from Sigma-Aldrich) at 301 mOsm. Recordings in current or voltage clamp modes were conducted to measure action potentials and membrane currents, respectively. For current-clamp recordings, the voltage response was evoked from a holding potential of −60 mV by applying current steps in 10 pA increments, each for 500 ms duration. For voltage-clamp recordings, cells were clamped at −60 mV and currents were evoked by voltage steps ranging from −80 to +60 mV in 10 mV increments and the peak current was measured.

2.12. Bioinformatic and statistical analysis

RNA sequencing reads were aligned to the ENSEMBL human reference genome (Homo_sapiens.GRCh37.75) and gene counts were generated using the STAR read aligner (Dobin et al., 2013). The Number of expressed transcripts in each cell line was defined as all transcripts with > 1 count detected (count > 1). Analysis of the count data to identify differentially expressed transcripts was performed using the DESeq2 package (Love et al., 2014). We also used DESeq2 to perform a time-series experiment using the likelihood ratio test to see whether the condition induces a change in gene expression during differentiation. A Benjamini-Hochberg adjusted *p*-value (p-adjusted) cut off of 0.05 was considered significant. To assess overall similarity between samples we calculate the Euclidean distance between samples using DESeq2. The functional annotations of differentially expressed genes (DEG) in DS cells compared to controls were identified using the web based annotation tools found in EnrichR (http://amp.pharm.mssm.edu/Enrichr/ (Wiki Pathways, ENCODE and ChEA Consensus TFs from ChIP-X; (Kuleshov et al., 2016). EnrichR was also used to detect similarities in expression patterns between our differentiated iPSCs and different brain regions (Human Gene Atlas (http://biogps.org/#goto=welcome) and Allen Brain Atlas (http://portal.brain-map.org/)).

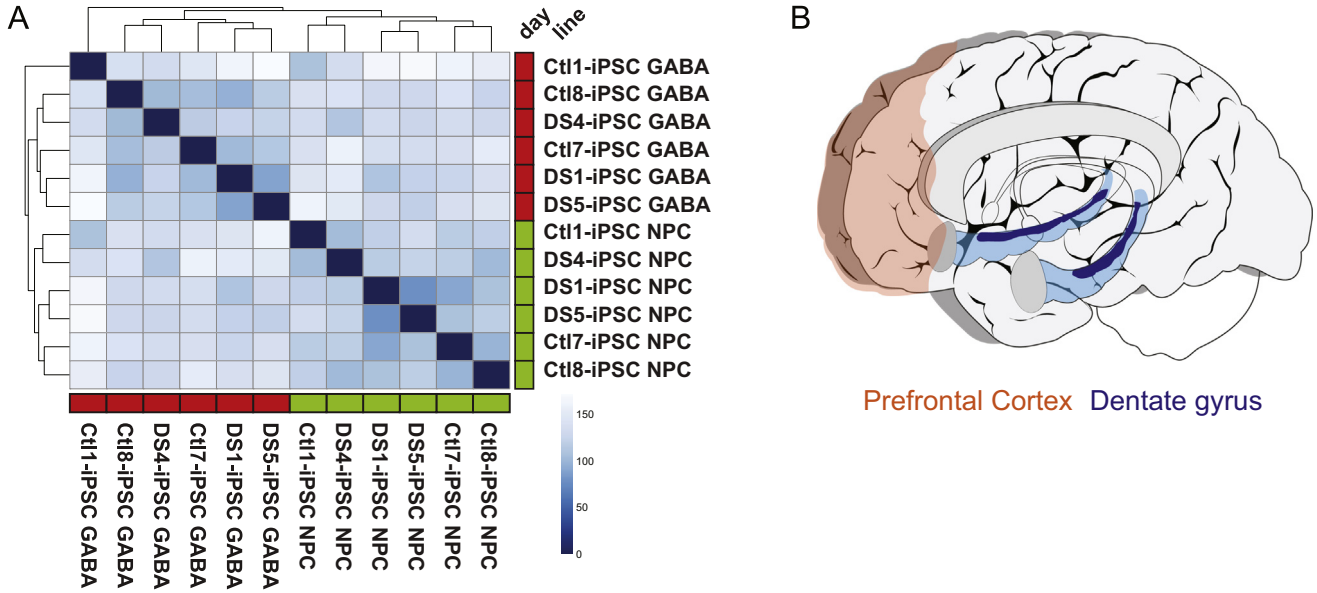

Fig. 2. Transcriptome profiles of iPSC neural derivatives show similarities to those from human brain regions relevant for DS.
A, Heatmap illustrating Euclidian distance of transcriptomes from neural lines with pathogenic *SCN1A* variants (DS1; DS5; DS5) and controls (Ctl1, Ctl7 and Ctl8) at d19 (iPSC NPC; green) and d65 (iPSC GABA; red) of differentiation. Transcriptomes cluster according to stage of differentiation and not to the *SCN1A* genotype (blue colour indicates similarities between samples, see scale bar). **B**, Schematic illustration of a section of human brain highlighting regions with transcriptome signatures similar to those in Ctl-iPSC GABA cells (brown, prefrontal cortex; blue, hippocampus with dentate gyrus in dark blue). The regions are important for e.g. executive functions, emotions, memory and cognition. (For interpretation of the references to colour in this figure legend, the reader is referred to the web version of this article.)

3. Results

3.1. DS-iPSC GABA cells show decreased sodium current density and altered voltage dependence

Pluripotency of patient derived induced pluripotent stem cell (DS-iPSC) clones carrying each of the heterozygous *SCN1A* variant was confirmed according to established criteria (Supplementary Fig. S1A–D). All DS-iPSC showed normal karyotypes from high-resolution G-banding. The DS-iPSC and Ctl-iPSC lines were matched for similar number of passages and then differentiated into neural progenitor cells (iPSC NPC) and GABAergic inter-neuronal (iPSC GABA) cells (Fig. 1A; Supplementary Fig. S2A). Immunostaining and quantitative real-time RT-PCR of iPSC NPC and iPSC GABA lines revealed neuronal cultures highly enriched for cells with a cortical interneuron identity (Maroof et al., 2013); Fig. 1C; Supplementary Fig. S2B). Expression of *SCN1A* and glutamate decarboxylase (*GAD*) was confirmed in neuronal cultures from d19 of differentiation (Supplementary Fig. S2B) and immunostaining confirmed that approximately 80% of neuronal cells were GABA-positive at d65 of differentiation in all cell lines (Fig. 1C).

Because *SCN1A* mutations reduce $Na_v1.1$ channel function, we assessed the electrophysiological properties in neuronal cells from d65. We performed whole-cell patch-clamp recordings on cells with a mature neuronal morphology (i.e. large and complex cell body, three or more neurites). The resting membrane potential generally ranged between −50 mV and −70 mV and the membrane capacitance was > 20 pF. In iPSC GABA cells derived from both controls and DS patients, action potentials were evoked in response to step current injections (Fig. 1D). The maximal frequency of the action potentials was significantly decreased in DS-iPS GABA cells (3.7 ± 1.1 Hz; $n = 6$) as compared to Ctl-iPSC GABA cells (9.7 ± 1.7 Hz; $n = 7$; p-value = .016, Student's t-test). When the activating current stimulus was 40 pA, the action potential frequency was 2.3 ± 0.3 Hz in DS ($n = 6$) and 7.4 ± 2.1 Hz in control cells ($n = 7$; p-value = .0513, Student's t-test). We further observed a shift of sodium current activation to more depolarized potentials in the three DS-iPSC GABA lines as compared to the three Ctl-iPSC GABA lines (Fig. 1E) suggesting *SCN1A* specific deficits in sodium currents. The detected shift in the maximal action frequency in the DS-iPSC GABA cells is in accord with the observed shift of the inward sodium current, disclosing biophysical impairments that recapitulate electrophysiological hallmarks of $Na_v1.1$ haploinsufficient interneurons.

3.2. DS-iPSC GABA cells show impaired response to oxidative stress

Several lines of evidence suggest oxidative stress to be a contributing factor in the pathophysiology of epilepsy (McElroy et al., 2017). In DS, seizures may be triggered by fever or external stimuli and we hypothesized that DS-iPSC GABA cells display increased sensitivity to cellular stress. We therefore measured the intracellular levels of reactive oxygen species (ROS) in d65 neuronal cell cultures enriched for GABAergic neurons, with and without hydrogen peroxide induction. Non-induced DS-iPSC GABA lines ($n = 3$) and Ctl-iPSC GABA lines ($n = 3$) displayed comparable levels of ROS (Fig. 1F). However, after adding hydrogen peroxide, the three DS-iPSC GABA lines exhibited a marked increase in levels of ROS compared to the Ctl-iPSC GABA lines (Fig. 1F; p-value < 0,05). This finding suggests impaired response to induced stress in DS-iPSC GABA cells.

3.3. Ctl-iPSC GABA cells display transcriptional profiles similar to brain regions relevant for Dravet syndrome

We assessed transcriptomes of DS-iPSC NPCs at d19 and of DS-iPSC GABA at d65 of differentiation ($n = 3$) and the corresponding cells from healthy subjects ($n = 3$) using strand sensitive RNA sequencing. We obtained on average 32 million reads in each sample (ranging from $25.5 * 10^6$ to $39.8 * 10^6$ reads), and we identified on average 28′169 and 25′947 expressed transcripts (counts > 1) in the samples at d19 and d65, respectively. The Euclidean distance between all samples ($n = 12$) was calculated from normalized expression data and samples clustered according to differentiation time points (Fig. 2A). This suggested that the overall transcriptome profiles of the iPSC NPCs and iPSC GABA are related primarily to degree of differentiation and not to the *SCN1A*

genotype.

Identification of relevant molecular perturbations in DS patient neural cells requires a system that generates transcriptome profiles from appropriate brain regions. To this end, we first assessed the composition of transcriptomes in Ctl-iPSC GABA at d65 and we compared the 3′000 most highly expressed genes with those across different brain regions in the Human Gene Atlas and the Allen Brain Atlas, respectively. Using EnrichR, we identified a strong overlap with brain regions termed "Prefrontal Cortex" and "Fetal Brain" (Human Gene Atlas) as well as "Dentate gyrus" and "Superficial dorsofrontal area" (Allen Brain Atlas; EnrichR combined score > 50; Fig. 2B). The prefrontal or dorsofrontal areas are highly interconnected parts of the prefrontal cortex involved in executive functions, memory and emotion (Lee and Worrell, 2012). These regions are relevant for cognition and different types of epilepsies (Lee and Worrell, 2012). The dentate gyrus is a structural part of the hippocampus that contains a significant number of inhibitory interneurons interconnected with other parts of the brain (Amaral et al., 2007). Furthermore, the dentate gyrus is of importance for cognition and the progression of ictal activity (Bui et al., 2018). These findings demonstrated that the Ctl-iPSC GABA cells yielded a transcriptional profile similar to that of brain regions relevant for DS.

3.4. Perturbed regulation of histone protein genes in differentiating neural cells with SCN1A variants

We then analyzed the three neural Ctl-iPSC lines for temporal changes in global transcriptomes between d19 (Ctl-iPSC NPC) and d65 (Ctl-iPSC GABA) of differentiation (Supplementary Fig. S3). Genes that were up-regulated ($n = 1210$) belonged to Wiki pathways for neuronal cell maturation (e.g. synaptic transmission and ion transport), while down-regulated genes ($n = 780$) belonged to Wiki pathways that are negatively associated with differentiation (e.g. cell cycle, DNA replication and chromatin remodeling; Supplementary Table S2 and Supplementary Table S3). This further supported that the iPSC GABA cells from healthy subjects represent mature and post-mitotic GABAergic neurons.

We hypothesized that $Na_v1.1$ haploinsufficiency interferes with gene expression and molecular pathways in a differentiation dependent manner. We therefore performed a time course analysis on transcriptome data obtained from the three DS-iPSC lines and the three Ctl-iPSC lines between d19 and d65. We identified altogether 14 transcripts that significantly changed expression in a condition-specific manner over time in the DS-iPSC neural lines when compared to iPSC neural lines from healthy subjects (adjusted p value < .05; Fig. 3A; Supplementary Table S4). In Ctl-iPSC neural lines, the 14 differentially expressed genes (DEGs) became markedly down-regulated between d19 and d65 whereas in DS-iPSC neural lines the same genes retained or increased their expression levels. Notably, 11 out of the 14 DEGs encode for histone proteins and another two DEGs, *UHRF1* and *BIRC5*, are important for histone ubiquitination (Kelly et al., 2010; Nishiyama et al., 2013) (Supplementary Table S4). Pathway analysis confirmed that these 13 DEGs belong to the Histone modification pathway (EnrichR and WikiPathway). The remaining DEG, *CEP55*, encodes a centrosomal protein of importance for mitotic exit (Fabbro et al., 2005).

To corroborate our findings and to identify additional transcriptional dysregulations in DS-iPSC neural cells with differentiation, we compared transcriptome data from the three DS-iPSC lines and the three Ctl-iPSC lines at either d19 or d65, respectively (Supplementary Fig. S3). At d19 we identified 26 DEGs (Supplementary Table S5) whereas at d65 of differentiation the number of DEGs increased to 171 DEGs (adjusted p-value < .05; Supplementary Table S6) of which 120 were expressed at a higher level in DS-iPSC GABA (Supplementary Fig. S3; Supplementary Table S6). Notably, 103 out of the 120 DEGs with higher expression in DS-iPSC at d65 belonged to a set of 780 genes that became down-regulated with differentiation in Ctl-lines (Fig. 3B, Supplementary Fig. S3; Supplementary Table S6). This indicates that the 103 genes, including the 14 DEGs identified from our time-course analysis, show retained or increased level of expression in DS-iPSC neural lines with differentiation as opposed to decreased expression in Ctl-iPSC neural lines. The DEGs at d19 and d65, respectively, were then investigated for clustering to biological functions. The analysis revealed that the DEGs in DS-iPSC GABA at d65, but not in DS-iPSC NPC at d19, were highly enriched in two pathways; Histone Modification (WP2369; adjusted p-value = 1.8 × 10–16) and Cell Cycle (WP179; adjusted p-value = 2.1 × 10–15; Fig. 3C; Supplementary Table S7).

The expression of histone genes is interconnected with cell cycle regulation (Almeida et al., 2018) and tightly regulated by 24 defined transcription factors (TFs; ENCODE and ChEA Consensus TFs from ChIP-X). We therefore investigated the expression of these up-stream TF genes in our data set and we found a marked up-regulation of *FOXM1* (adjusted p-value = 3.7×10^{-27}) and *E2F1* (adjusted p-value = 1.5×10^{-5}) in all DS-iPSC GABA cells (Fig. 3C; Supplementary Table S6). The two TFs are positive regulators of 44 out of the 103 up-regulated genes belonging to the disrupted Histone Modification and Cell Cycle pathways in DS-iPSC GABA (Supplementary Table S8). Finally, 51 genes among the 171 DEGs identified at d65 showed reduced expression in DS-iPSC GABA cells when compared to control; and two of these genes belong to the Glutathione metabolism pathway (WP100; Supplementary Fig. S3; Supplementary Tables S6–S7). Taken together, our findings disclose an increasing number of DEGs in DS-iPSC neural cells with differentiation into GABAergic cells, predominantly because of retained or increased expression levels. The DEGs are highly enriched for genes encoding histones, histone modifiers and proteins important for the cell cycle, suggesting global effects on the chromatin architecture with neural differentiation. Furthermore, we identified an up-regulation of the genes encoding the two transcription factors FOXM1 and E2F1 as likely contributors to the perturbed pathways for histone modification and cell cycle regulation (Fig. 3A–C; Supplementary Table S7).

3.5. Co-dysregulation of genes for epilepsy and neural plasticity in DS-iPSC neural cells

Besides the transcriptional alterations emerging with differentiation in neural lines carrying *SCN1A* variants, we sought to investigate if any genes were dysregulated in DS-iPSC at both d19 and d65 of differentiation. We found ten genes with a sustained dysregulation in DS-iPSC neural lines when compared to Ctl-iPSC neural lines (Fig. 3D–E). The genes included one antisense transcript, five long non-coding RNA (lncRNA) genes and four protein-coding genes (*DPP6*, *GSTM1*, *LYNX1* and *ZXDA*; Fig. 3D–E). Notably, three out of the four dysregulated protein coding genes have a strong connection to neuronal functions relevant for DS. First, the *DPP6* gene, encoding Dipeptidyl peptidase VI, was markedly downregulated (log2 fold change −9.7). The protein is important for excitability and synaptic long-term potentiation and has previously been associated with neurodevelopmental delay (Maussion et al., 2017) and impaired learning in mice (Lin et al., 2018). Second, the *GSTM1* gene, encoding Glutathione S-transferase of importance for oxidative stress control (Liu and Tsai, 2002), was down-regulated (log2fold change −6.4). *GSTM1* gene variants have previously been associated with seizures (Chbili et al., 2014). Finally, *LYNX1*, encoding Ly6/neurotoxin, was strongly up-regulated (log2fold change 9.2). The protein restricts plasticity of mature cortical networks (Morishita et al., 2010). The four dysregulated lncRNAs and the antisense transcript have not been studied in detail and the role for these particular transcripts in neuronal function and neurodevelopment are yet unclear. Further studies are required to clarify the specific functions of these RNAs (Ayana et al., 2017; Clark and Blackshaw, 2014; Koreman et al., 2018; Yao and Jin, 2014). These results indicate a preserved co-dysregulation of a small set of genes in both DS-iPSC NPCs and DS-iPSC GABA cells. Three of these genes are previously associated with neurodevelopment, seizures or neural plasticity, suggesting complex functional perturbations

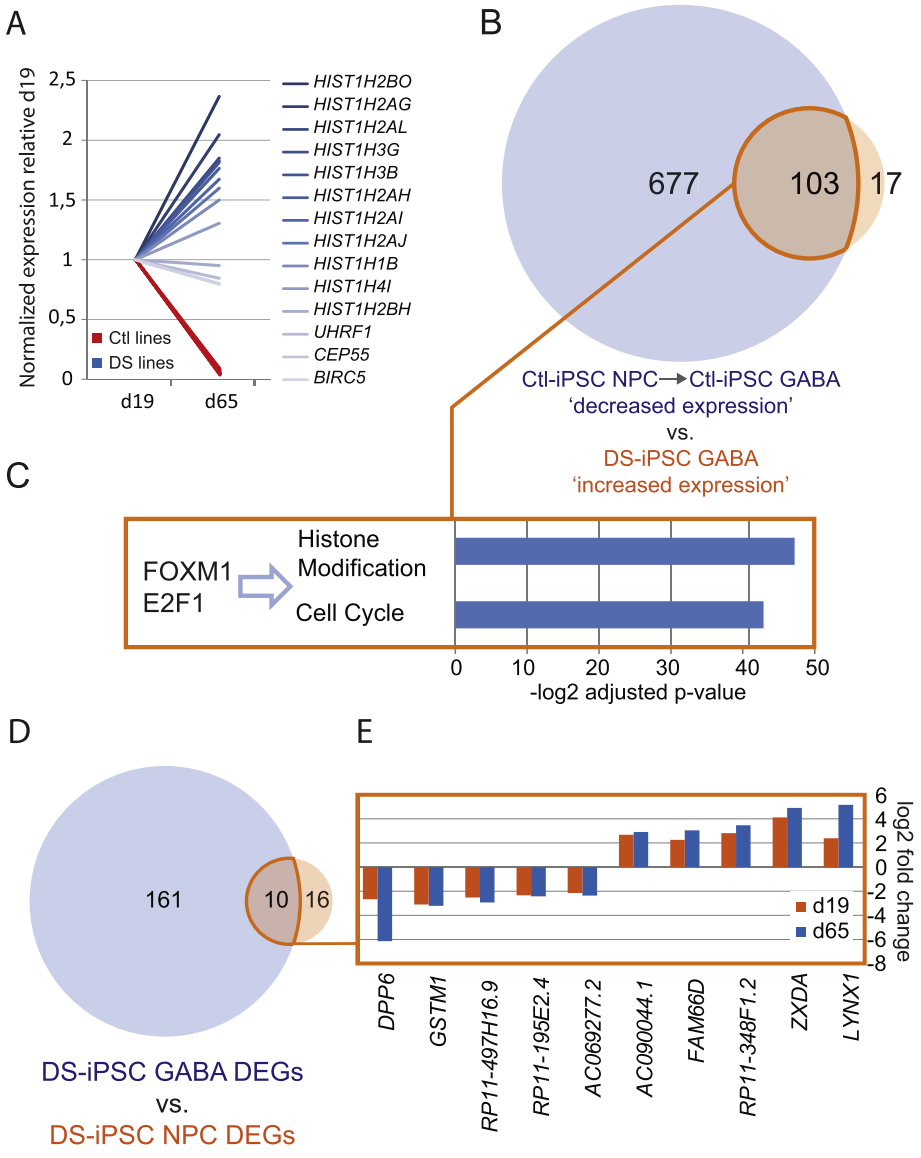

Fig. 3. Dysregulation of genes for chromatin architecture, cell cycle and neuronal function in DS-iPSC with *SCN1A* variants.
A, Time course experiment comparing transcriptomes from iPSC NPC at d19 and iPSC GABA at d65 of neural differentiation in *SCN1A* haploinsufficient (DS; $n = 3$) and control (Ctl) lines ($n = 3$). Fourteen genes show a distinct and condition specific decrease in expression in Ctl-iPSC lines (red lines) whereas the *SCN1A* haploinsufficient lines show retained or increased expression levels (blue lines). Expression of genes (counts) is shown relative that at d19 (*HIST1H*(n), Histone genes; *UHRF1*, Ubiquitin like with PHD and Ring Finger Domains 1; *CEP55*, Centrosomal Protein 55; *BIRC5*, Baculoviral IAP Repeat Containing 5). **B**, Venn diagram illustrating the number of genes that are downregulated during differentiation in Ctl-iPSC neural cells (Ctl-iPSC NCP ➔ Ctl-iPSC GABA 'decreased expression'; blue circle, $n = 780$) and the overlapping proportion (orange line; $n = 103$) of genes showing a relative increase in expression in neuronal cells with pathogenic *SCN1A* variants (DS-iPSC GABA 'increased expression'; orange circle, $n = 120$). The majority of DEGs ($n = 103$) in DS-iPSC GABA lines at d65 show retained or increased expression levels between d19 and d65. **C**, Diagram showing the enrichment of pathways for Histone modification and Cell Cycle (Wiki Pathways) after analysis of the 103 DEGs with relative increase in expression in DS-iPSC GABA cells. Both pathways are regulated by the transcription factors FOXM1 and E2F1 having increased expression in DS-iPSC GABA cells. The relative increase of expression of the two TFs in DS-iPSC GABA cells is indicated ($-\log2$ adjusted p-value). **D**, Venn diagram illustrating 26 DEGs at d19 (orange circle) and 171 DEGs at d65 (blue circle) when comparing transcriptomes from DS-iPSC and Ctl-iPSC neural cell lines. Ten genes (orange line) were differentially expressed in DS-iPSC neural cells at both d19 and d65 of differentiation. **E**, Boxed graph showing 10 DEGs that are dysregulated at both d19 (orange bars) and d65 (blue bars) of differentiation in DS-iPSC lines vs. Ctl-iPSC lines (log2 fold change). The *DPP6* (Dipeptidyl Peptidase Like 6), *GSTM1* (Glutathione S-Transferase Mu 1) and *LYNX1* (Ly6/Neurotoxin 1) genes are previously associated with specific neuronal functions relevant for DS. (*ZXDA*, Zinc Finger X-Linked Duplicated A; lincRNA genes: *RP11-497H16.9*, *RP11-195E2.4*, *AC069277.2*, *AC090044.1*; antisense RNA gene: *FAM66D*). (For interpretation of the references to colour in this figure legend, the reader is referred to the web version of this article.)

in $Na_v1.1$ haploinsufficient iPSC neural derivatives that are relevant for DS.

4. Discussion

In this study, we established iPSCs from skin fibroblasts of three DS patients carrying distinct heterozygous *SCN1A* variants. The DS-iPSC lines and three iPSC lines derived from healthy donors were subsequently differentiated into neural cell cultures highly enriched for GABAergic neurons, the cell type primarily affected in DS. The significance of our model for neurodevelopment in DS was assessed by transcriptome analysis from GABAergic neuronal cultures showing a global gene expression pattern similar to that of "Prefrontal Cortex", "Fetal Brain", "Dentate gyrus" and "Superficial dorsofrontal area", brain regions that are relevant for clinical features in DS. Furthermore, we detected electrophysiological abnormalities in the DS-iPSC GABA lines carrying *SCN1A* variants consistent with a decreased sodium current density and an impaired excitability of inhibitory interneurons, previously reported in a DS mouse model (Tai et al., 2014). These combined findings suggest that our neural iPSC lines are suitable for exploration of neuropathophysiological mechanisms in DS.

We tested our DS model for response to oxidative stress with and without hydrogen peroxide (H_2O_2) induction. The analysis revealed increased ROS levels in our DS-iPSC GABA lines after H_2O_2 induction when compared to Ctl-iPSC GABA cells. Elevated ROS levels and escalated oxidative stress have been reported in models of temporal lobe epilepsy with memory deficits (TLE; (Pearson et al., 2015). Interestingly, pharmacological removal of ROS attenuated the cognitive symptoms. In DS, independent reports have documented cases with *SCN1A* mutations showing atypical neurological sequelae following status epilepticus (Okumura et al., 2012; Tang et al., 2011). Our study shows that the $Na_v1.1$ haploinsufficient iPSC GABA cells are more vulnerable to induced stress and the increased ROS levels may suggest a contributing mechanism to neuronal cell damage in DS.

We performed a comprehensive analysis of gene expression in iPSC derived GABAergic lines from DS patients and healthy subjects that brings novel aspects for further understanding of the molecular perturbations in $Na_v1.1$ haploinsufficient interneurons. The transcriptome profiles of differentiating, GABAergic and $Na_v1.1$ haploinsufficient cells uncovered an enrichment of dysregulated genes of importance for

chromatin assembly and cell cycle regulation. In addition, the study identified three continuously co-dysregulated genes in DS-iPSC neural cells previously associated with epilepsies, cognitive deficit and aberrant neuronal plasticity.

The co-dysregulation of the genes *GSTM1* and *DPP6*, previously associated with excitability, and at two differentiation time points in our DS model, adds to prior findings of a shared gene regulatory network in epilepsies (Delahaye-Duriez et al., 2016; Noebels, 2015). The reduced expression of the epilepsy gene *GSTM1,* important for oxidative stress control and ROS clearance that alleviate seizures (Liu and Tsai, 2002), is also consistent with our observed increase in ROS levels in stress induced DS-iPSC GABA cells. This finding supports an impaired response to cellular stress in $Na_v1.1$ haploinsufficient cells as a potentially contributing factor in the pathophysiology of DS (McElroy et al., 2017). Variants in the *DPP6* gene have previously been associated with neurodevelopmental delay (Maussion et al., 2017) and *Dpp6* null mice show impaired learning and memory (Lin et al., 2018). The marked down-regulation of *DPP6* in $Na_v1.1$ haploinsufficient GABAergic cells may thus suggest one link to the cognitive deficit in DS. We further identified an up-regulation of *LYNX1* encoding a protein that inhibits nicotinic *n*-acetylcholine receptor activity (Miwa et al., 1999). The LYNX1 protein restricts plasticity of mature cortical networks resulting in disturbed neuronal connectivity and synaptic functions (Morishita et al., 2010). The increased *LYNX1* expression is thus compatible with perturbation of neural circuitries in the developing brain mediated by $Na_v1.1$ haploinsufficient cells.

Unexpectedly, the transcriptome analysis revealed a marked and dynamic dysregulation of pathways for histone modifications and cell cycle regulation in the DS-iPSC neural lines. These two interconnected pathways were altered in DS-iPSC GABA cells at d65, but not in DS-iPSC NPC at d19 from our time course analysis. The expression of histone protein genes was markedly increased in DS-iPSC neuronal lines as opposed to down-regulation in control iPSC lines. Histones and histone modifications are essential for cell proliferation and transcriptional control as well as for the temporal dynamics of gene expression regulating neural cell fate specification, commitment and differentiation (Gao et al., 2014; Lilja et al., 2013; Park et al., 2014). Furthermore, chromatin remodeling is a prerequisite for the plasticity of neural networks throughout development that is specific for brain regions and age (Broccoli et al., 2015; Gao et al., 2014; Park et al., 2014). Since the initial discovery of pathogenic variants in genes encoding chromatin remodelers and chromatin components behind disrupted brain development (Amir et al., 1999; Gibbons et al., 1995), an expanding number of neurodevelopmental disorders are now associated with perturbations of chromatin architecture and histone modifications (Kleefstra et al., 2014; Larizza and Finelli, 2019). Increased histone protein levels and altered histone stoichiometry have been shown to disturb histone deposition and chromatin structure in dividing cells (Lacoste et al., 2014). This provides a mechanistic model by which altered levels of histones may contribute to perturbed neurogenesis in $Na_v1.1$ haploinsufficient cells.

Histone protein genes are transcribed in the S-phase and tightly coordinated with DNA replication (Kurat et al., 2014). In addition to the marked upregulation of histone protein genes in our study, we found increased levels of *CEP55*, important for mitotic exit (Fabbro et al., 2005), *BIRC5*, promoting chromosome segregation and proliferation (Kelly et al., 2010), and *UHRF1*, important for G1/S transition (Nishiyama et al., 2013). This observation indicates a disturbed cell cycle progression in differentiating GABAergic cells carrying pathogenic *SCN1A* variants. Interestingly, the dysregulation of pathways for histone modifications and cell cycle regulation in differentiating neural cells is accompanied by an up-regulation of the TF genes *FOXM1* and *E2F1*. Both TFs are positive regulators of the 14 “core” genes that are strongly up-regulated between d19 and d65. FOXM1 targets critical genes regulating the G2/M phases of the cell-cycle whereas E2F1 functions in the progression from G1 to S phase (Fischer et al., 2016). The two TFs are seemingly complementary in targeting critical genes of importance for cell cycle progression and their up-regulation is consistent with the dysregulated pathways for histone modification and cell cycle in our model of DS neurogenesis.

Although seizure is a predominant feature in DS, cognitive impairment appears to develop independently (Brunklaus and Zuberi, 2014; Gataullina and Dulac, 2017, 2018) and possibly related to distinct $Na_v1.1$ haploinsufficient cell populations that do not mediate ictal activities. The human GABAergic system develops during the second half of gestation into infancy (Xu et al., 2011) and forms numerous connections with other neuronal subtypes in the cortex that are pivotal in controlling neural circuitries of the central nervous system (Kepecs and Fishell, 2014). In rodents, at least 20 different GABAergic inter-neuronal subtypes are described with distinct morphology, connectivity and biophysical properties (Kelsom and Lu, 2013). Furthermore, the effects of GABAergic transmission vary with neuronal development (Galanopoulou, 2007). Given the functional heterogeneity of GABAergic interneurons, the different transcriptional changes disclosed in our study may hypothetically, and possibly in combination, result in a plethora of neurodevelopmental perturbations. While our model shows extensive promise for further understanding of molecular mechanisms behind perturbed neurogenesis in DS, the protocol to generate forebrain neural cells and GABAergic interneurons in particular, may underestimate the molecular alterations in vivo because of the reduced heterogeneity in our cultured cell populations. Further investigations of $Na_v1.1$ haploinsufficiency in functionally distinct interneuronal cell populations are now required to clarify the molecular background to different neurological features associated with DS. More complex models of human neural differentiation using e.g. 3D organoids, build up by a mixture of cell types, followed by single cell transcriptome analysis may add to our findings.

5. Conclusion

We established DS patient iPSC GABAergic cells with $Na_v1.1$ haploinsufficiency displaying characteristic electrophysiological abnormalities and impaired response to induced cellular stress. Using transcriptome analysis, we show that genes for chromatin components, chromatin modifications and cell cycle regulators are markedly dysregulated and emerge with differentiation from DS-iPSC NPC to DS-iPSC GABAergic cells. Furthermore, we show that DS-iPSC neural cells exhibit co-dysregulated genes of importance for neuronal plasticity, excitability and connectivity. The combined findings highlight candidate genes and processes for perturbed neurodevelopment in DS that overlap with mechanisms behind neurodevelopmental disorders. The data provide a framework to identify and test biological mechanisms underlying the neuropathophysiology and the complex clinical features in DS.

Supplementary data to this article can be found on-line.

Supplementary data to this article can be found online at https://doi.org/10.1016/j.nbd.2019.104583.

Author contributions

Conceptualization, J.S. and N.D.; Methodology and Investigation, J.S., L.L., F.H.N. and M.S.; Formal Analysis, J.S., L.L., J.K., Z.J., S.V.K., M.H., B.B. and N.D.; Visualization, J.S., L.L. and J.K.; Writing – Original Draft, J.S. and L.L.; Writing – Review & Editing, J.S., J.K., B.B. and N.D.; Supervision, J.S., B.B. and N.D.; Funding Acquisition, B.B. and N.D. All authors approved the final version of the manuscript.

Declaration of Competing Interest

This research was conducted in the absence of any commercial or financial relationships that could be construed as a potential conflict of interest.

Acknowledgements

We thank participants and their families for cooperation. This work was supported by grants from the Swedish Research Council (2015-02424 to ND; 2015-02417 to BB), Sävstaholm Society, AstraZeneca, Hjärnfonden (FO2018-0100 and FO2019-0210 to ND), Uppsala University and Science for Life Laboratory. L.L. was funded by grants from the Sävstaholm Society and her contributions were independent of support from AstraZeneca. M.H. was financially supported by the Knut and Alice Wallenberg Foundation as part of the National Bioinformatics Infrastructure Sweden at SciLifeLab. The transcriptomes were generated at the SNP&SEQ platform, Imaging was performed at the BioVis Platform and scorecard processing at the Genome Centre platform, Science for Life Laboratory, Uppsala University. Computations were performed on resources provided by SNIC through Uppsala Multidisciplinary Center for Advanced Computational Science (UPPMAX). We thank F. Schwarz and V. Sequeira for excellent technical support. The funders played no role in study design, data collection and interpretation or decision to publish.

References

Akiyama, M., et al., 2010. A long-term follow-up study of Dravet syndrome up to adulthood. Epilepsia. 51, 1043–1052.
Almeida, R., et al., 2018. Chromatin conformation regulates the coordination between DNA replication and transcription. Nat. Commun. 9, 1590.
Amaral, D.G., et al., 2007. The dentate gyrus: fundamental neuroanatomical organization (dentate gyrus for dummies). Prog. Brain Res. 163, 3–22.
Amir, R.E., et al., 1999. Rett syndrome is caused by mutations in X-linked MECP2, encoding methyl-CpG-binding protein 2. Nat. Genet. 23, 185–188.
Ayana, R., et al., 2017. Decoding crucial LncRNAs implicated in neurogenesis and neurological disorders. Stem Cells Dev. 26, 541–553.
Bechi, G., et al., 2012. Pure haploinsufficiency for Dravet syndrome Na(V)1.1 (SCN1A) sodium channel truncating mutations. Epilepsia. 53, 87–100.
Broccoli, V., et al., 2015. Histone modifications controlling native and induced neural stem cell identity. Curr. Opin. Genet. Dev. 34, 95–101.
Brunklaus, A., Zuberi, S.M., 2014. Dravet syndrome–from epileptic encephalopathy to channelopathy. Epilepsia. 55, 979–984.
Bui, A.D., et al., 2018. Dentate gyrus mossy cells control spontaneous convulsive seizures and spatial memory. Science. 359, 787–790.
Catarino, C.B., et al., 2011. Dravet syndrome as epileptic encephalopathy: evidence from long-term course and neuropathology. Brain. 134, 2982–3010.
Catterall, W.A., et al., 2010. NaV1.1 channels and epilepsy. J. Physiol. 588, 1849–1859.
Chbili, C., et al., 2014. Effects of glutathione S-transferase M1 and T1 deletions on epilepsy risk among a Tunisian population. Epilepsy Res. 108, 1168–1173.
Chopra, R., Isom, L.L., 2014. Untangling the Dravet syndrome seizure network: the changing face of a rare genetic epilepsy. Epilepsy Currents. 14, 86–89.
Clark, B.S., Blackshaw, S., 2014. Long non-coding RNA-dependent transcriptional regulation in neuronal development and disease. Front. Genet. 5, 164.
Delahaye-Duriez, A., et al., 2016. Rare and common epilepsies converge on a shared gene regulatory network providing opportunities for novel antiepileptic drug discovery. Genome Biol. 17, 245.
Depienne, C., et al., 2009. Spectrum of SCN1A gene mutations associated with Dravet syndrome: analysis of 333 patients. J. Med. Genet. 46, 183–191.
Dobin, A., et al., 2013. STAR: ultrafast universal RNA-seq aligner. Bioinformatics. 29, 15–21.
Dravet, C., et al., 2005. Severe myoclonic epilepsy in infancy: Dravet syndrome. Adv. Neurol. 95, 71–102.
Dravet, C., et al., 2011. Severe myoclonic epilepsy in infancy (Dravet syndrome) 30 years later. Epilepsia. 52 (Suppl. 2), 1–2.
Fabbro, M., et al., 2005. Cdk1/Erk2- and Plk1-dependent phosphorylation of a centrosome protein, Cep55, is required for its recruitment to midbody and cytokinesis. Dev. Cell 9, 477–488.
Fischer, M., et al., 2016. Integration of TP53, DREAM, MMB-FOXM1 and RB-E2F target gene analyses identifies cell cycle gene regulatory networks. Nucleic Acids Res. 44, 6070–6086.
Galanopoulou, A.S., 2007. Developmental patterns in the regulation of chloride homeostasis and GABA(A) receptor signaling by seizures. Epilepsia. 48 (Suppl. 5), 14–18.
Gao, Z., et al., 2014. An AUTS2-Polycomb complex activates gene expression in the CNS. Nature. 516, 349–354.
Gataullina, S., Dulac, O., 2017. From genotype to phenotype in Dravet disease. Seizure. 44, 58–64.
Gataullina, S., Dulac, O., 2018. Is epilepsy the cause of comorbidities in Dravet syndrome? Dev. Med. Child Neurol. 60, 8.
Gibbons, R.J., et al., 1995. Mutations in a putative global transcriptional regulator cause X-linked mental retardation with alpha-thalassemia (ATR-X syndrome). Cell. 80, 837–845.
Harkin, L.A., et al., 2007. The spectrum of SCN1A-related infantile epileptic encephalopathies. Brain. 130, 843–852.
Higurashi, N., et al., 2013. A human Dravet syndrome model from patient induced pluripotent stem cells. Mol. Brain. 6, 19.
Jiao, J., et al., 2013. Modeling Dravet syndrome using induced pluripotent stem cells (iPSCs) and directly converted neurons. Hum. Mol. Genet. 22, 4241–4252.
Jin, Z., et al., 2011. GABA-activated single-channel and tonic currents in rat brain slices. J. Vis. Exp.(53).
Kalume, F., et al., 2015. Sleep impairment and reduced interneuron excitability in a mouse model of Dravet syndrome. Neurobiol. Dis. 77, 141–154.
Katayama, Y., et al., 2016. CHD8 haploinsufficiency results in autistic-like phenotypes in mice. Nature. 537, 675–679.
Kelly, A.E., et al., 2010. Survivin reads phosphorylated histone H3 threonine 3 to activate the mitotic kinase Aurora B. Science. 330, 235–239.
Kelsom, C., Lu, W., 2013. Development and specification of GABAergic cortical interneurons. Cell Biosci. 3, 19.
Kepecs, A., Fishell, G., 2014. Interneuron cell types are fit to function. Nature. 505, 318–326.
Kleefstra, T., et al., 2014. The genetics of cognitive epigenetics. Neuropharmacology. 80, 83–94.
Koreman, E., et al., 2018. Chromatin remodeling and epigenetic regulation of oligodendrocyte myelination and myelin repair. Mol. Cell. Neurosci. 87, 18–26.
Kuleshov, M.V., et al., 2016. Enrichr: a comprehensive gene set enrichment analysis web server 2016 update. Nucleic Acids Res. 44, W90–W97.
Kurat, C.F., et al., 2014. Regulation of histone gene transcription in yeast. Cell. Mol. Life Sci. 71, 599–613.
Lacoste, N., et al., 2014. Mislocalization of the centromeric histone variant CenH3/CENP-A in human cells depends on the chaperone DAXX. Mol. Cell 53, 631–644.
Larizza, L., Finelli, P., 2019. Developmental disorders with intellectual disability driven by chromatin dysregulation: clinical overlaps and molecular mechanisms. Clin. Genet. 95, 231–240.
Lee, R.W., Worrell, G.A., 2012. Dorsolateral frontal lobe epilepsy. J. Clin. Neurophysiol. 29, 379–384.
Lilja, T., et al., 2013. Like a rolling histone: epigenetic regulation of neural stem cells and brain development by factors controlling histone acetylation and methylation. Biochim. Biophys. Acta 1830, 2354–2360.
Lin, L., et al., 2018. DPP6 loss impacts hippocampal synaptic development and induces behavioral impairments in recognition, learning and memory. Front. Cell. Neurosci. 12, 84.
Liu, C.S., Tsai, C.S., 2002. Enhanced lipid peroxidation in epileptics with null genotype of glutathione S-transferase M1 and intractable seizure. Jpn. J. Pharmacol. 90, 291–294.
Lorincz, A., Nusser, Z., 2010. Molecular identity of dendritic voltage-gated sodium channels. Science. 328, 906–909.
Love, M.I., et al., 2014. Moderated estimation of fold change and dispersion for RNA-seq data with DESeq2. Genome Biol. 15, 550.
Maeda, H., et al., 2016. Establishment of isogenic iPSCs from an individual with SCN1A mutation mosaicism as a model for investigating neurocognitive impairment in Dravet syndrome. J. Hum. Genet. 61, 565–569.
Maroof, A.M., et al., 2013. Directed differentiation and functional maturation of cortical interneurons from human embryonic stem cells. Cell Stem Cell 12, 559–572.
Maussion, G., et al., 2017. Implication of LRRC4C and DPP6 in neurodevelopmental disorders. Am. J. Med. Genet. A 173, 395–406.
McElroy, P.B., et al., 2017. Scavenging reactive oxygen species inhibits status epilepticus-induced neuroinflammation. Exp. Neurol. 298, 13–22.
Miwa, J.M., et al., 1999. lynx1, an endogenous toxin-like modulator of nicotinic acetylcholine receptors in the mammalian CNS. Neuron. 23, 105–114.
Morishita, H., et al., 2010. Lynx1, a cholinergic brake, limits plasticity in adult visual cortex. Science. 330, 1238–1240.
Nishiyama, A., et al., 2013. Uhrf1-dependent H3K23 ubiquitylation couples maintenance DNA methylation and replication. Nature. 502, 249–253.
Noebels, J., 2015. Pathway-driven discovery of epilepsy genes. Nat. Neurosci. 18, 344–350.
Okumura, A., et al., 2012. Acute encephalopathy in children with Dravet syndrome. Epilepsia. 53, 79–86.
Park, D.H., et al., 2014. Activation of neuronal gene expression by the JMJD3 demethylase is required for postnatal and adult brain neurogenesis. Cell Rep. 8, 1290–1299.
Pearson, J.N., et al., 2015. Reactive oxygen species mediate cognitive deficits in experimental temporal lobe epilepsy. Neurobiol. Dis. 82, 289–297.
Rooney, D., Czepulkowski, B., 1992. Human Cytogenetics. A Practical Approach. Oxford University Press.
Scheffer, I.E., et al., 2009. Dravet syndrome or genetic (generalized) epilepsy with febrile seizures plus? Brain Dev. 31, 394–400.
Schuster, J., et al., 2015. Transcriptome profiling reveals degree of variability in induced pluripotent stem cell lines: impact for human disease modeling. Cell Rep. 17, 327–337.
Sobol, M., Raykova, D., Cavelier, L., Khalfallah, A., Schuster, J., Dahl, N., 2015. Methods of reprogramming to iPSC associated with chromosomal integrity and delineation of a chromosome 5q candidate region for growth advantage. Stem Cells Dev. 24, 2032–2040.
Sun, Y., et al., 2016. A deleterious Nav1.1 mutation selectively impairs telencephalic inhibitory neurons derived from Dravet syndrome patients. Elife 5.
Symonds, J.D., et al., 2017. Advances in epilepsy gene discovery and implications for epilepsy diagnosis and treatment. Curr. Opin. Neurol. 30, 193–199.
Tai, C., et al., 2014. Impaired excitability of somatostatin- and parvalbumin-expressing cortical interneurons in a mouse model of Dravet syndrome. Proc. Natl. Acad. Sci. U. S. A. 111, E3139–E3148.
Tang, S., et al., 2011. Encephalopathy and SCN1A mutations. Epilepsia. 52, e26–e30.
Tebbenkamp, A.T., et al., 2014. The developmental transcriptome of the human brain: implications for neurodevelopmental disorders. Curr. Opin. Neurol. 27, 149–156.
Xu, G., et al., 2011. Late development of the GABAergic system in the human cerebral cortex and white matter. J. Neuropathol. Exp. Neurol. 70, 841–858.
Yao, B., Jin, P., 2014. Unlocking epigenetic codes in neurogenesis. Genes Dev. 28, 1253–1271.
Yu, F.H., et al., 2006. Reduced sodium current in GABAergic interneurons in a mouse model of severe myoclonic epilepsy in infancy. Nat. Neurosci. 9, 1142–1149.